Investigation of the Crystallization Stages of LTA-Type Zeolite by Complementary Characterization Techniques

Monique Smaihi,*[a] Olivier Barida,[a] and Valentin Valtchev[b]

Keywords: Zeolites / Hydrothermal synthesis / NMR spectroscopy / Crystal growth

This paper reports on the physicochemical reorganizations, at 40 °C, of a template-free aluminosilicate system yielding an LTA-type zeolite. The events that take place in the system during the transformations of the amorphous material into a crystalline material were monitored by various characterization techniques which provide information from the molecular to the micrometer scale. High-resolution solid-state ^{29}Si and ^{27}Al MAS NMR spectroscopy, small-angle X-ray scattering (SAXS), X-ray diffraction (XRD), and scanning electron microscopy (SEM) were used in order to achieve a better understanding of the structural properties of the precursor gel and its transformation into a crystalline zeolite-type material. The experimental results show that the first crystallization stage proceeds by reorganization of the amorphous aluminosilicate units formed during the mixing of the precursors. This reorganization involves an ordering of the Si–O–Al bond angles and operates on aggregates of constant volume. The crystallization process takes place in the volume of the aggregates by propagation through the gel phase. This propagation through the gel continues to complete the transformation of the particles into crystalline zeolite Na-A nanocrystals with a rough surface. After this stage, the growth in the system is dominated by the solution-mediated transport, which leads to the formation of well-shaped zeolite A crystals.

Introduction

Zeolites are crystalline solids that have a highly regular and open microporous structure.[1] More than 130 microporous structure types are known,[2] each with its own distinct pore size, shape, and interconnectivity. The sizes of these pore openings range from 0.3 to 1 nm. The framework composition (Si/Al ratio) can give rise to different ion-exchange properties, to a hydrophilic or hydrophobic character of the material, and to acid sites with different strengths and densities.

Owing to its excellent ion-exchange capacity and consequent use as a water-softening agent in modern-day washing powders, zeolite A boasts the greatest world-wide industrial tonnage of any zeolite. Besides the important industrial applications, zeolite A attracts the interest of researchers with its relatively simple composition and fast crystallization kinetics, which makes it very useful for fundamental studies.

Many techniques have been used to gain an insight into the complex processes occurring during the nucleation and subsequent crystal-growth processes.[3−26] Recently, the use of various non-intrusive and in-situ techniques have provided evidence to support the theory of zeolite crystallization through gel transformation, even for situations considered before as homogeneous.[20,22] The presence of aluminosilicate nanoparticles in the early stages of nucleation of zeolite A has been confirmed by quasi-elastic light scattering and SAXS,[11] dynamic light scattering (DLS),[17,18] TEM,[8] and AFM.[7,14] SAXS observations[19−21] have suggested that some physical rearrangements occur within the amorphous aluminosilicate particles during the nucleation process. A number of studies on the transformations occurring on a molecular scale during the nucleation and crystal-growth processes were based on Nuclear Magnetic Resonance (NMR) spectroscopy.[22−25] Such a spectroscopic method is complementary to those presented above; it fills the gaps in the information needed between the molecular scale entities and the crystal structure formed. Several studies[23−26] showed how the initial reactant sources greatly affect the intermediates observed during the crystallization process. These investigations showed the complexity of the zeolite nucleation/crystallization process, which is dependent on the overall composition of the initial system and the silica and alumina sources used.

Although it was proven that the nucleation of zeolite A is related to the presence of aluminosilicate gel, many questions concerning different stages of evolution of the system remain to be met. The crystal growth can take place by propagation through the gel phase or by solution-mediated transport. In a particular reaction system, the true mechanism could lie somewhere between these two extremes, where one of those might be dominant at a certain stage. In

[a] IEM, UMR 5635, CNRS,
1919 route de Mende, 34293 Montpellier Cedex 5, France
[b] LMM, UMR 7016, CNRS, ENSC Mulhouse, Université de Haute Alsace,
3 rue Alfred Werner, 68093 Mulhouse Cedex, France

  DOI: 10.1002/ejic.200300154

order to highlight the mechanism that controls the zeolite formation in a particular system, a link between events taking place on an atomic and on a large scale has to be established. Therefore, valuable information on the mechanism governing crystal growth could be obtained only by a combination of methods which provide information from the molecular to the micrometric scale.

The goal of the present study was to distinguish different stages of zeolite A formation at low temperature, and to investigate the mechanism controlling each of these stages for a conventional organic-free system. The experiments were performed at 40 °C in order to slow down crystal growth so as to distinguish different stages of zeolite formation. High-resolution solid-state ^{29}Si and ^{27}Al MAS NMR spectroscopy, SAXS, X-ray diffraction (XRD), and scanning electron microscopy (SEM) were used to provide information from the molecular to the micrometer scale, and thus to achieve a better understanding of the structural properties of the solid gel phase and its transformation into a crystalline LTA-type material.

Results

The XRD patterns of the samples after different crystallization times are shown in Figure 1. Traces of crystalline LTA-type material were detected after 14 h of hydrothermal synthesis, whereas after 16 h, the XRD pattern showed all the characteristic peaks of zeolite A. A gradual increase in the crystallinity was observed between 14 and 20 h. Further increase in the synthesis time did not yield material with higher X-ray crystallinity.

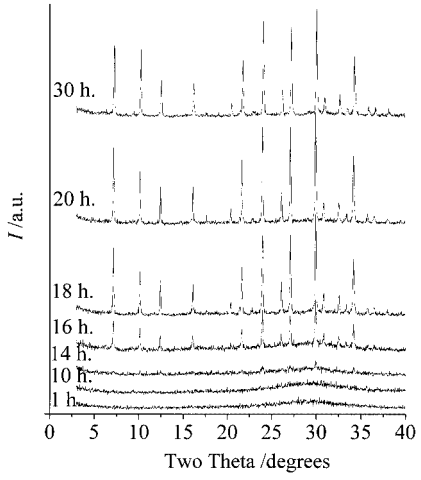

Figure 1. X-ray diffractograms of samples prepared at 40 °C for various heating times: a) 1 h; b) 10 h; c) 14 h; d) 16 h; e) 18 h; f) 20 h; g) 30 h

The electron micrographs shown in Figure 2 represent the morphological features of the materials taken after 1, 16, and 20 h of hydrothermal treatment. The micrograph of the material taken after 1 h shows that the material does not have a crystalline appearance. However, isometric particles of similar sizes, which form large aggregates can be seen. The sizes of these primary particles are in the range 40−100 nm. The micrograph of the sample taken after 16 h shows isolated particles with a round shape and sizes from 40 to 300 nm. All samples that were treated hydrothermally for more than 18 h contained crystals that are of similar sizes, with cubic morphology typical of zeolite A. The sizes of the crystals are in the range 300−400 nm. A small fraction of 40−100 nm crystallites can also be seen.

The morphologies and interfaces of the samples crystallized for different periods of time were characterized by SAXS. The SAXS data provide information on the presence of different particle populations, and on some of their properties such as particle-size distribution, their shape and the type of interactions they are involved in. The intensity of the small-angle X-ray scattering, $I(Q)$, is given by the general equation

$$I(Q) = \varphi P(Q)S(Q)$$

where φ is the number density of the particles in the sample and Q is the momentum transfer [$Q = 4\pi\cdot\lambda^{-1}\cdot\sin(\theta/2)$, θ the scattering angle, λ the X-ray wavelength]. The form factor $P(Q)$ reflects the distribution of the scattering material in the scattering particle, and the structure factor $S(Q)$ is related to the spatial distribution of the scattering particles in the material. The relation between a scattering spectrum and the species responsible for the scattering is shown schematically in Figure 3. On the scale of the primary building units (Porod region, $QR_g >> 1 >> Qa$, where a is the monomer size), the form factor of the primary building units becomes dominant in the scattering pattern, thus providing information about the surface structure of these particles. In many cases, the concept of fractal geometry[27] is used to describe scattering curves in the Porod region. Basi-

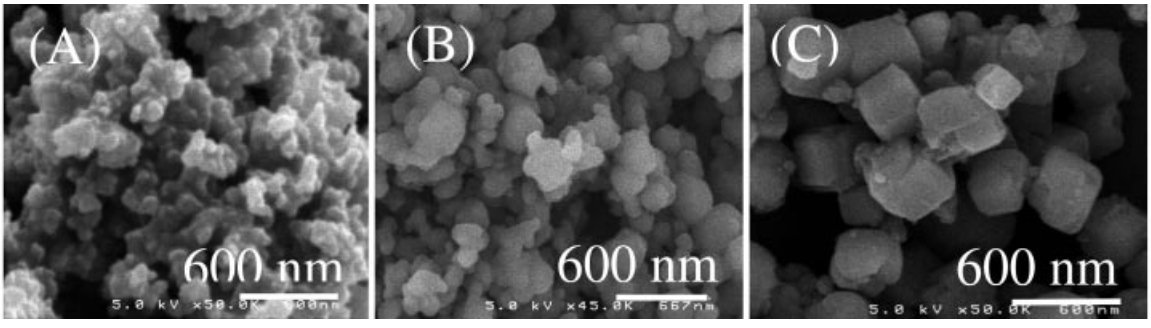

Figure 2. SEM micrographs of samples prepared at 40 °C for various heating times: (A) 1 h; (B) 16 h; (C) 20 h

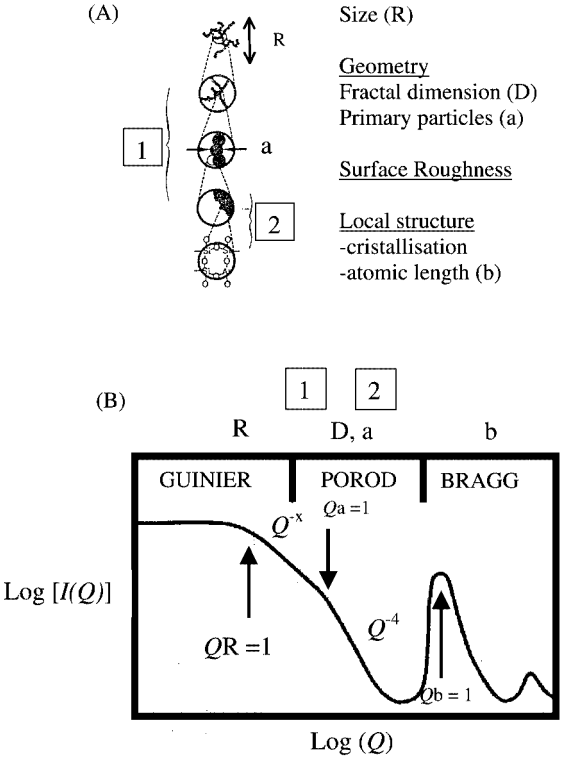

Figure 3. Relation between a scattering spectrum and the species responsible for the scattering: A) aggregate structure at various scales; B) scattering profile of the aggregates presented in A) (according to ref.[34])

cally, all fractals show a power law dependence of the scattered intensity I on the scattering vector Q: $I(Q) \propto Q^{-x}$. For 3-dimensional objects with fractal surfaces,[28] $x = 6 - D_s$, where D_s is the fractal dimension of the surface ($2 \leq D_s \leq 3$). D_s provides a quantitative measure of the roughness; if the roughness of the surface increases, D_s will increase. Thus, $D_s = 2$ represents a classical smooth surface. The $I(Q)$ curves (Figure 4) are similar for all samples with slopes ranging from -3.8 (± 0.05) for samples with "short" synthesis time (1−14 h) to -4 (± 0.05) for those obtained after

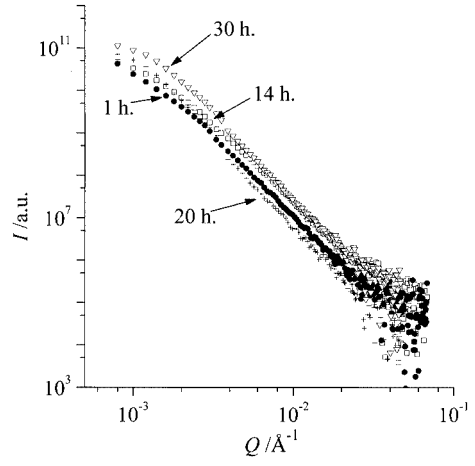

Figure 4. SAXS profiles of samples obtained after different synthesis times at 40 °C

20−30 h of thermal treatment. The initial decay of the intensity in the Guinier region also varies slightly with hydrothermal treatment of the samples.

The molecular organization in the samples was studied by ^{29}Si and ^{27}Al NMR spectroscopy. The ^{29}Si NMR and ^{27}Al NMR spectra of the precursor solutions were recorded in order to characterize the initial species before mixing. Each spectrum presents a single line at $\delta = -72.2$ and 79.5 ppm, which are assigned to the monomeric $Si(OH)_4$ and $Al(OH)_4^-$ species, respectively. The ^{29}Si and ^{27}Al NMR chemical shifts (δ) and line-widths ($\Delta\nu_{1/2}$) recorded for all solid samples are summarized in Table 1. The ^{29}Si MAS NMR spectra of samples obtained after a short synthesis time exhibit broad signals between $\delta = -78$ and -92 ppm (Figure 5). Sample 1 (Table 1) presents a relatively broad signal (half-width = 668 Hz) with a chemical shift of the peak maximum at $\delta = -83.5$ ppm. With increasing synthesis time, the resonance signal becomes narrower and also shows a change in the chemical shift distribution. After 8 h of synthesis, the resonance signal is centered at $\delta = -85.9$ ppm, and after 14 h of thermal treatment, an additional shoulder appears at $\delta = -88.4$ ppm. The latter increases with synthesis time at the expense of the higher frequency resonances. After 20 h of synthesis, the spectrum presents a single narrow signal centered at $\delta = -89.5$ ppm, which does not change with further thermal treatment. The ^{27}Al MAS NMR spectra have been recorded using the same samples (Figure 6). They all present a single signal centered at $\delta = +58$ ppm. The width of this resonance signal then decreases with the time of thermal treatment. The spectrum collected after 1 h of synthesis presents a broad signal (half-width = 1197 Hz), whereas the spectrum recorded after 20 h presents a narrow signal (half-width = 400 Hz) which does not change with further thermal treatment.

Discussion

The TEM study of the initial gel showed that the 40−100 nm particles formed non-uniform gel aggregates (Figure 7). The large-scale changes observed by SEM show that aggregates composed of nanoparticles with a random form are seen in the system during the induction period. The characteristic morphological features of the product did not change substantially after 14 h of hydrothermal treatment, when traces of crystalline LTA-type material were detected in the XRD pattern of the product. In the sample crystallized for 16 h, which displayed a relatively high crystallinity (approximately 30%) (Figure 2, B), particles without the specific morphological features of LTA-type zeolite were observed. All these data show that the first stage of the crystallization process is not coupled with substantial morphological changes in the solid. This result could be considered as reasonable if the crystallization takes place in the volume of the gel phase. Bearing in mind the mass of the crystallites at this stage, and the fact that the density of the zeolite and the gel is about 2.0 and 1.0,

Table 1. ^{29}Si and ^{27}Al NMR spectroscopic data of the samples obtained after 1−30 h of hydrothermal treatment at 40 °C

Sample	Reaction time at 40 °C [h]	δ(Si) [ppm] (±0.1)	$\Delta\nu_{1/2}$(Si) [ppm] (±5%)	δ(Al) [ppm] (±0.1)	$\Delta\nu_{1/2}$(Al) [ppm] (±5%)	Nature of the solid
1	1	−83.5	668	57.9	1197	amorphous
2	8	−85.9	668	58.4	1271	amorphous
3	14	−83.5/−88.4	802	57.7	1152	amorphous > LTA
4	16	−89.5	99.3	58.5	556	LTA > amorphous
5	18	−89.2	69	58.6	477	LTA
6	20	−89.5	74	58.3	387	LTA
7	30	−89.4	136	58.4	451	LTA

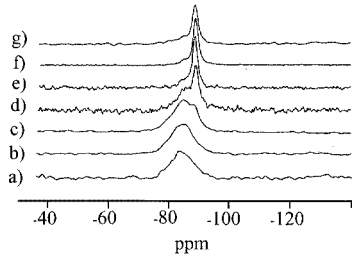

Figure 5. ^{29}Si MAS NMR spectra of samples obtained after different synthesis times at 40 °C: a) 1 h; b) 10 h; c) 14 h; d) 16 h; e) 18 h; f) 20 h; g) 30 h

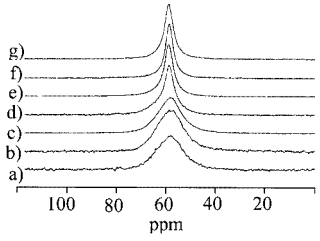

Figure 6. ^{27}Al MAS NMR spectra of samples obtained after different synthesis times at 40 °C: a) 1 h; b) 10 h; c) 14 h; d) 16 h; e) 18 h; f) 20 h; g) 30 h

respectively, a substantial decrease in the volume could not be expected. On the other hand, if the zeolite nuclei are released by the gel phase and grown in the mother liquor, at 30% conversion, the formation of new particles would be observed in the product.

Complementary information on the morphological changes in the course of the transformation of the initial gel into crystalline zeolite A was obtained by the SAXS investigation. From the initial decay of the SAXS intensity in the Guinier region, the electronic radius of gyration, Rg, can be deduced using the Guinier approximation for scattering particles $I(Q) = N{\cdot}n^2{\cdot}\exp(-Q^2{\cdot}\mathrm{Rg}^2/3)$, where N is the number density of particles and n the number of excess electrons in each particle.

The Guinier radius (Figure 8) is about 100 nm and does not drastically vary with the time of thermal treatment. In spite of the limitations of the Guinier method due to the restricted Q range and the possible interference effects due to multiple particle scattering, the obtained values for samples that were heated for up to 20 h are not unreason-

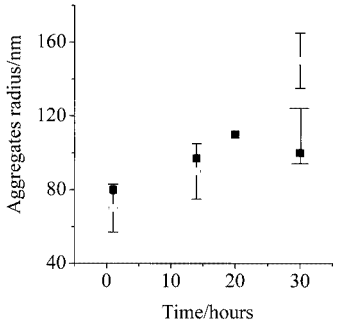

Figure 8. Aggregates radius obtained from SAXS profiles (solid squares), SEM micrographs (open circles) as a function of heating time at 40 °C

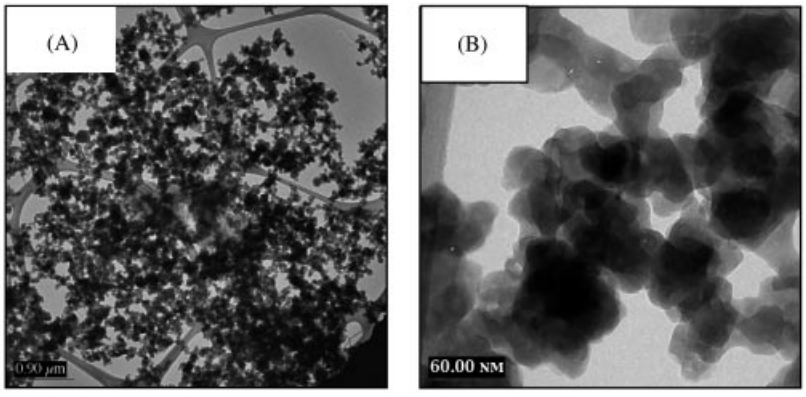

Figure 7. Low (A) and high (B) magnification TEM images of the zeolite A precursor gel

able and the estimated errors are ±10 nm. For crystalline samples (30 h of thermal treatment), the restricted Q range of the experimental set-up may underestimate the Guinier radius of particles larger than 250 nm, and leads to larger experimental errors (±30 nm). However, the sizes observed by SEM are consistent with the Guinier radii for all samples treated for up to 30 h, and similarly do not significantly vary during the first 14 h of thermal treatment.

Porod plots for all samples (Figure 4) show a single region with a slope of about −3.8 for the noncrystalline samples and −4 for the crystalline samples. The SAXS profiles observed for all samples are rather similar and insensitive to the crystallization stage. The observed Porod slopes of about −4 indicate that the particle surfaces are smooth. Several studies have been devoted to the characterization of silicate networks obtained under different conditions, and show that the scattering curves display fractal dimensions varying from −2 to −4 depending on the polymerization conditions.[28b,28c] Further, with regard to the specific case of zeolite crystallization, there have been many studies involving the crystallization of silicalite under different conditions.[29] Slopes observed during crystallization of these systems ranged between −2 and −4, depending on the composition of the system and the aging of the system.

In our case, it can be concluded that the SAXS investigation is in agreement with the SEM observation, i.e. on the morphological scale there were no changes during the first stage of zeolite formation. In other words, as the SAXS measurements did not detect the formation of new particles, the nucleation and the subsequent growth of the nuclei takes place in the volume of the gel. Thus, it appears that the nucleation and subsequent crystallization occur with aggregates of constant size. A close association of the initially formed nuclei with the gel particles has already been described by Gora et al.[17] However, it is difficult, to discuss the transport of the nutrient during this stage.

On a molecular scale amorphous highly disordered species were detected during this stage. The broad resonance observed between δ = −78 and −92 ppm in the ^{29}Si MAS NMR spectra of sample 1 is typical of amorphous aluminosilicates.[30] This broadness is mainly caused by the overlapping of individual peaks with slightly different δ values, due to the small differences in the structural arrangements in the SiO_4 tetrahedra of the gel skeleton. The ^{29}Si and ^{27}Al NMR spectra of aluminosilicate solutions, pertinent to zeolite synthesis, indicate the formation of Si−O−Al linkages by the appearance of up to four peaks assigned to the Al(OSi), $Al(OSi)_2$, $Al(OSi)_3$, and $Al(OSi)_4$ species.[31] For solid samples, characteristic ^{29}Si NMR chemical shift ranges for the five $Q^4(m\text{Al})$ [i.e. $Si(OSi)_{4-m}(OAl)_m$] units in framework silicates have been established by comparison between calculated and experimental chemical shifts.[32] They range from δ = −112 to −94 ppm for $1 \leq m \leq 4$. Thus, the presence of such units in our samples can be excluded. Further, hydroxylated units, such as $HOSi(OAl)_3$, for which chemical shift values may be expected in the range of the observed signal, should be present only in minor amounts since no noticeable signal enhancement is observed in the ^{1}H-^{29}Si cross-polarization spectrum.

For sample 6 (20 h, 40 °C), the chemical shift of δ = −89.5 ppm reveals that the framework of the gel consists mainly of $Si(OAl)_4$ building units, i.e. of silicon atoms linked by oxygen bridges to four tetrahedral aluminum atoms. This chemical shift is consistent with the presence of crystalline zeolite Na-LTA (Si/Al = 1).[33]

Since the ^{29}Si NMR spectra can be analyzed quantitatively (the total area of the peaks corresponds to 100% of the observed nuclei), the signal centered at δ = −89.5 ppm corresponding to $Si(OAl)_4$ units in crystalline Na-A zeolite can be deconvoluted from the spectra in order to follow the kinetics of the formation of these units. Figure 9 presents the proportion of $Si(OAl)_4$ crystalline units as a function of crystallization time. This curve shows an "induction" period of about 10 h, which precedes a steep rise. After 20 h of synthesis (t/t_c = 1), 95% of the silicon species are $Si(OAl)_4$ crystalline units. Nevertheless, an increase in the size of the crystals and the formation of crystals with well-defined crystal morphology was observed after this period.

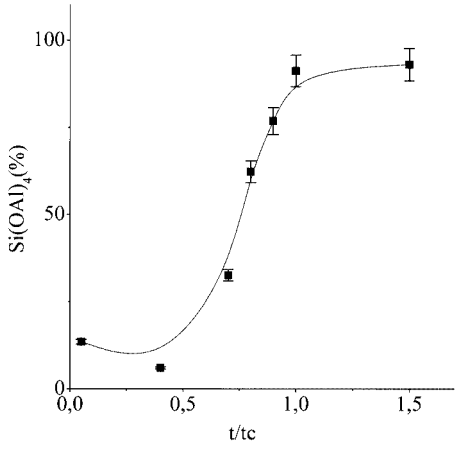

Figure 9. Proportion of crystalline $Si(OAl)_4$ units as a function of crystallization time (t_c: time needed to obtain pure crystalline Na-A zeolite)

The single signal centered at δ = +58 ppm in the ^{27}Al MAS NMR spectra is typical of $Al(OSi)_4$ units. The highly symmetrical line shape indicates that the presence of hydroxylated AlO_4 species is unlikely. Moreover, no signals corresponding to octahedral AlO_6 or tetrahedral $Al(OAl)_4$ aluminate species are detected. For the latter two units, ^{27}Al NMR chemical shifts of δ ≈ 0 and +75 ppm, respectively, were found in previous studies.[34] The observed line broadening is probably caused by residual quadrupolar interactions due to slight symmetry distortions in the vicinity of the Al atoms. However, these quadrupolar interactions are small enough such that they do not modify the line shape.

Short-range ordering in the samples can also be estimated from the line-widths of the ^{29}Si and ^{27}Al NMR resonance signals. The most likely contributing factor to the line-width ($\Delta\nu_{1/2}$) is the structural disorder which involves

a large number of slightly different environments around nominally equivalent $Q^n(m\text{Al})$ type silicon atoms, thus leading to many overlapping lines with slightly different chemical shifts. The different environments are created by distortion of bond angles and bond lengths due to lattice imperfections. Hence, very broad signals ($\Delta\nu_{1/2} \approx 10-20$ ppm) are observed for highly disordered systems such as amorphous materials, whereas narrow peaks ($\Delta\nu_{1/2} \approx 0.2-3$ ppm) are obtained for perfectly ordered systems. Figure 10 presents the evolution of the ^{29}Si and ^{27}Al MAS NMR signal line-width as a function of the synthesis time for the $Si(OAl)_4$ and $Al(OSi)_4$ species. Both curves present two regions where a slight decrease in the line-width is observed for up to 14 h, followed by a significant decrease in the line-width after 16 h of synthesis.

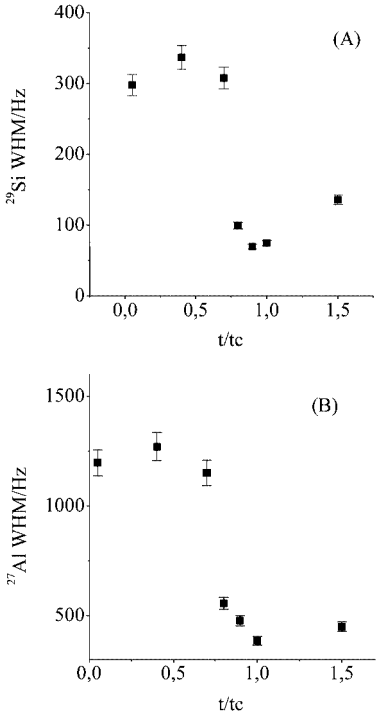

Figure 10. Width at half maximum of the $Si(OAl)_4$ (A) and $Al(OSi)_4$ (B) resonance signals of the ^{29}Si and ^{27}Al MAS NMR spectra, respectively, as a function of crystallization time at 40 °C (t_c: time needed to obtain pure crystalline Na-A zeolite)

Thus, the information collected on the molecular scale shows that during the first 16 h, while no large-scale morphological changes were observed, the first crystallization stage involves a rearrangement of the Si−O−T bonds in the amorphous phase formed after precursor mixing prior to crystallization. After this induction period when a product with zero crystallinity was observed, the above-mentioned transformation in the system takes place. This stage includes the time period 12−16 h, when the increase in the crystallinity is not coupled with large-scale changes in the system, i.e. the crystalline particles retain the size and morphology of the initial amorphous gel precursors. Obviously, during this first stage, the dominant mechanism of crystal growth is propagation through the gel. Growth by propagation through the gel network has already been observed in the formation of zeolite L.[16] During this first stage, the solid is about 30% crystalline, according to the XRD measurements (Figure 1). The nutrients for the crystal growth are provided mainly by the amorphous gel phase, although an extensive exchange between the solid and liquid parts of the system is likely.

After the first stage, a very rapid increase in crystallinity was observed which was coupled with significant changes in the size and morphological features of the particles. Well-shaped zeolite A crystals in the product indicate a change in the crystal growth process. This distinct change in the system occurred during the period 16−18 h, when the crystallinity is about 50%. At this stage, a substantial part of the amorphous material is consumed and crystallites are either released by the gel or are in contact with the mother liquor.[34] The SEM study of the 18-h product does not show much material with an amorphous appearance. At this stage the product already contains well-distinguished individual particles. During this latter stage, a solution-mediated growth mechanism seems to be dominant in the system. This crystallization stage, where a layer growth mechanism controls the zeolite A formation, has been studied and described in detail by Agger et al.[7] The nutrients for this crystallization stage are provided by the amorphous part of the gel and the less stable zeolite nanoparticles. The crystallization during this second stage was completed between 16 and 20 h, and further hydrothermal treatment did not influence the morphology nor the crystallinity of the product. The disappearance of the small crystallites and the increase in the size of the well-shaped cubic crystals were observed during the 20−30-h period, thus resembling Ostwald ripening.

Conclusions

The present study reports on the results obtained during the formation and transformations of precursor particles for the whole course of the template-free Na-A zeolite crystallization process at 40 °C, using various characterization techniques that provide information from the molecular to the micron scale.

The experimental results showed that in the system under investigation the crystallization process could be subdivided into two stages, during which the crystallization process is controlled by different crystallization mechanisms. After the formation of viable nuclei, the first stage of the crystal growth process proceeded by reorganization of the amorphous homogeneous aluminosilicate phase formed during the mixing of the initial precursors. This reorganization involves an ordering of the Si−O−Al bond angles of the $Si(OAl)_4$ units and operates on aggregates of constant volume to form nanocrystals with a rough surface at the end of the process. The zeolite formation in the system was

completed by the second crystallization stage when a fully crystalline product containing well-shaped zeolite crystals was obtained. A layer growth, where a solution-mediated transport of nutrients dominates, is the controlling mechanism during the second stage.

Experimental Section

Samples Preparation: The Na-A zeolite samples were prepared from an initial gel with the following composition: $7.5Na_2O/0.5Al_2O_3/SiO_2/200H_2O$. Sodium silicate solution (overall composition $SiO_2/7.5NaOH/102H_2O$) was prepared by dissolving sodium silicate (2.22 g, $Na_2Si_3O_7$, 27% SiO_2, 17% NaOH, Aldrich) and sodium hydroxide (2.69 g) in H_2O (17.1 g). A sodium aluminate solution (overall composition $Al_2O_3/15NaOH/197H_2O$) was prepared by dissolving sodium aluminate (0.963 g, $NaAlO_2$, 53% Al_2O_3, 42% Na_2O, Riedel−de Haën) and sodium hydroxide (2.465 g) in H_2O (17.69 g). The solutions were stirred in closed polyethylene bottles at room temperature until complete dissolution of the solid. After mixing of the initial solutions, the resultant mixture was stirred vigorously for 15 min. During mixing, the solution became opaque. The syntheses were performed at 40 °C for different periods of time ranging from 1 to 30 h. At this temperature, the crystallization of the zeolite A was relatively slow, but still fast enough to be achieved in a reasonable period of time. The solid phase was recovered after 5−8 cycles of centrifugation (8000 rpm, 15 min), decanting and ultrasonic redispersion in distilled water. The solid phase was dried over silica gel at room temperature for 48 h. The yield based on the silica conversion was ca. 70%. A similar (slightly higher) yield (76%) was obtained in the reference experiment performed with the same initial system at 90 °C for 5 h.

Samples Characterization: Scanning electron micrographs were obtained with a Hitachi S-4500 microscope. All samples were platinum-coated (2−3 nm) and mounted on aluminum mounts with carbon conducting tape. X-ray diffraction measurements were performed with a Bruker diffractometer D-5000 (Cu-$K_{\alpha 1}$ radiation, 0.154 nm). Small-angle X-ray scattering experiments were performed with an instrument that has an incident wavelength of 0.154 nm (Cu-$K_{\alpha 1}$ radiation) using a high-resolution Bonse-Hart camera. The monochromator was a three-reflection channel-cut scattered beam. These experimental parameters allow studies in a range of wave vectors Q from 0.02 to 1 nm^{-1}. The ^{29}Si and ^{27}Al NMR spectra of the precursor solutions were obtained at 49.68 and 65.17 MHz, respectively, with a Bruker spectrometer. The ^{29}Si spectra were recorded using a 12-μs pulse width (corresponding to a 60° flip angle), 10 s pulse repetition time and 128 scans. The ^{27}Al spectra were recorded using a 4-μs pulse width (corresponding to a 45° flip angle), 0.1 s pulse repetition time and 256 scans. The ^{29}Si MAS NMR spectra of the solid samples were recorded with a Bruker spectrometer at 39.73 MHz, using 4-μs single pulses (60° flip angle) with 60 s repetition rate, and employing high-power proton decoupling and magic-angle spinning at 3.5 kHz; 1000 scans were accumulated. The powder samples were filled into zirconia rotors of 4 mm diameter. The ^{27}Al MAS NMR spectra were measured at 104.26 MHz, using single pulses of 1 μs duration with 1 s repetition rate, and employing magic-angle spinning at 10 kHz; 512 scans were accumulated. All ^{27}Al and ^{29}Si chemical shifts were referenced to a 1% aqueous $Al(H_2O)_6^{3+}$ solution and tetramethylsilane (TMS), respectively.

Acknowledgments

The authors thank Dr. H. Kessler for helpful discussions and D. Cot for the SEM micrographs.

[1] R. M. Barrer, *Zeolites and Clay Minerals and Sorbents and Molecular Sieves*, Academic Press, New York, **1978**.
[2] W. M. Meier, D. H. Olson, *Atlas of Zeolite Structure Types*, 3rd ed., Butterworth-Heinemann, London, **1992**.
[3] S. P. Zhdanov, in: *Molecular Sieve Zeolites* (Eds.: E. M. Flanigen, L. B. Sand), Adv. Chem. Ser. 101, ACS, Washington, DC, **1971**, p. 20−43.
[4] R. J. Francis, D. O'Hoare, *J. Chem. Soc., Dalton Trans.* **1998**, 3133−3148.
[5] A. K. Cheetham, C. F. Mellot, *Chem. Mater.* **1997**, *9*, 2269−2279.
[6] M. E. Davis, R. F. Lobo, *Chem. Mater.* **1992**, *4*, 756−768.
[7] J. R. Agger, N. Pervaiz, A. K. Cheetham, M. W. Anderson, *J. Am. Chem. Soc.* **1998**, *120*, 10754−10759.
[8] S. Mintova, N. H. Olson, V. Valtchev, T. Bein, *Science* **1999**, *283*, 958−960.
[9] R. I. Walton, R. I. Smith, D. O'Hare, *Microporous Mesoporous Mater.* **2001**, *48*, 79−88.
[10] Y. Marui, R. Irie, H. Takiyama, H. Uchida, M. Matsuoka, *J. Cryst. Growth* **2002**, 237−239, 2148−2152.
[11] P. S. Singh, T. L. Dowling, J. N. Watson, J. M. White, *Phys. Chem. Chem. Phys.* **1999**, *1*, 4125−4130.
[12] R. Grizetti, G. Artioli, *Microporous Mesoporous Mater.* **2002**, *54*, 105−112.
[13] V. Nikolakis, D. G. Vlacho, M. Tsapatsis, *Microporous Mesoporous Mater.* **1998**, *21*, 337−346.
[14] S. Sugiyama, S. Yamamoto, O. Matsukoa, H. Noroye, J. Yu, G. Zhu, S. Qiu, O. Terasaki, *Microporous Mesoporous Mater.* **1999**, *28*, 1−7.
[15] M. Smaihi, S. Kallus, J. D. F. Ramsay, *Stud. Surf. Sci. Catal.* **2001**, *135*, 183.
[16] M. Tsapatsis, M. Lovallo, M. E. Davis, *Microporous Mater.* **1996**, *5*, 381−388.
[17] L. Gora, K. Streletzky, R. W. Thompson, G. D. J. Phillies, *Zeolites* **1997**, *18*, 119−131.
[18] B. J. Schoeman, O. Regev, *Zeolites* **1996**, *17*, 447−456.
[19] P. W. J. G. Wijnen, T. P. M. Beelen, R. A. Van Santen, in: *The Colloidal Chemistry of Silica*, Advances in Chemistry Series, **1994**, vol. 234, p. 517.
[20] W. H. Dokter, H. F. Van Garderen, T. P. M. Beelen, R. A. Van Santen, W. Bras, *Angew. Chem. Int. Ed. Engl.* **1995**, *34*, 73−75.
[21] O. Regev, Y. Cohen, E. Kehat, Y. Talmon, *Zeolites* **1994**, *14*, 314−319.
[22] S. L. Burkett, M. E. Davis, *J. Phys. Chem.* **1994**, *98*, 4647−4653.
[23] G. Engelhardt, B. Fahlke, M. Mägi, E. Lippmaa, *Zeolites* **1985**, *5*, 49−52.
[24] J. Shi, M. W. Anderson, *Chem. Mater.* **1996**, *8*, 369−375.
[25] G. Engelhardt, B. Fahlke, M. Mägi, E. Lippmaa, *Zeolites* **1983**, *3*, 292−294.
[26] S. Mintova, V. Valtchev, *Microporous Mesoporous Mater.* **2002**, *55*, 171−179.
[27] B. B. Mandelbrot, *Fractals, Form and Chance*, Freeman, San Francisco, **1977**.
[28] [28a] H. D. Bale, P. W. Schmidt, *Phys. Rev. Lett.* **1984**, *53*, 596−599. [28b] D. W. Schaeffer, K. D. Keefer, *Fractals in Physics* (Eds.: L. Pietronero, E. Tosatti), Elsevier B. V., Amsterdam, **1986**, p. 39−45. [28c] D. W. Schaeffer, K. D. Keefer, *Phys. Rev. Lett.* **1984**, *53*, 1383−1386.
[29] P. P. E. A. de Moor, T. P. M. Beelen, R. A. van Santen, *Microporous Mater.* **1997**, *9*, 117−130.
[30] E. Lipmaa, A. Mägi, A. Samoson, M. Tarmak, G. Engelhardt, *J. Am. Chem. Soc.* **1981**, *103*, 4992−4996.

[31] L. S. Dent-Glasser, G. Harvey, *Proceedings of the 6th International Zeolite Conference* (Reno, 1983), Butterworth, Guildford, **1985**, p. 925.
[32] J. M. Bennett, C. S. Blaskwell, D. F. Fox, *J. Phys. Chem.* **1983**, *87*, 3783−3790.
[33] G. Engelhardt, D. Michel, *High-Resolution Solid State NMR of Silicates and Zeolites* John Wiley & Sons, New York, **1987**.
[34] S. Gontier, L. Gora, I. Güray, R. W. Thompson, *Zeolites* **1993**, *13*, 414−418.

Received March 24, 2003
Early View Article
Published Online October 10, 2003

